Quadrupolar electromagnetic field from detonation of high explosive charges on the ground surface

S. P. Soloviev

Institute of Geospheres Dynamics, Moscow, Russia

V. V. Surkov

Moscow State Engineering Physics Institute, Moscow, Russia

J. J. Sweeney

Lawrence Livermore National Laboratory, Livermore, California, USA

[1]   Experimental results of a study of electromagnetic fields due to detonation of high explosive charges with mass of a few kilograms are presented in this paper. Data show that in the initial stage of explosion the fields decrease as the fourth power of distance. Such a quadrupolar type of field contradicts the concept that an explosion is characterized by an effective electric dipole. A theoretical analysis is given based on expansion of an electromagnetic field in multipole moments. The theory is used to make estimates of the quadrupolar and dipole moments of the electric charge system resulting from an explosion occurring at the Earth's surface; calculations of electric fields thus produced are similar to those observed.   *INDEX TERMS:* 0619 Electromagnetics: Electromagnetic theory; 0684 Electromagnetics: Transient and time domain; 0694 Electromagnetics: Instrumentation and techniques; 7219 Seismology: Nuclear explosion seismology; *KEYWORDS:* chemical explosion, electromagnetic fields, quadrupolar, electric dipole, experimental

1.   Introduction

[2]   Experiments designed to observe electromagnetic signals from explosions show that a low-frequency electromagnetic field is created by an explosion [*Adushkin and Soloviev*, 1996; *Adushkin et al.*, 1990; *Boronin et al.*, 1990a, 1990b, 1973; *Brovkin et al.*, 1990; *Cook*, 1959; *Gorshunov et al.*, 1967; *Gertcenshtein and Sirotinin*, 1970; *Kolsky*, 1954; *Martner and Sparks*, 1959; *Sweeney*, 1989]. All data to date have been recorded at distances considerably less than the characteristic wavelength of the electromagnetic wave; that is, these data meet the near field requirement. High explosive charges during the experiments [*Boronin et al.*, 1990a, 1990b, 1973; *Gorshunov et al.*, 1967] were placed in the air at a height of several meters from the ground or were placed on a metal or dielectric plate [*Kolsky*, 1954]. Only the vertical component of the electric field was measured during these experiments by passive electric antennas. The magnetic field during these experiments was not studied. The recording of electric field was carried out, at most, only at two separate distances from the explosive charge. On the basis of the ratio of the magnitudes of the signals measured at only two different points, *Boronin et al.* [1990b] made a conclusion about distance dependence of the electric field. These previous studies suggest that the amplitude of the recorded electric signal decreases as $\sim r^{-3}$. Therefore, as a rule for estimating field

strength at large distances, the system of electric charges formed by a chemical explosion has been characterized as an electric dipole.

[3]   It should be noted that if the typical size, R_0, of the explosive cloud at the time of signal maximum (for example, $R_0 \sim 1$ m for the explosive mass of 0.66 kg used by *Boronin et al.* [1973]) was of the same order as the distance between explosive point and electric antennas ($r \sim 1.5$–3.5 m, used in the same study), the signal characteristics might depend on the size of the space charge and its distribution within the explosive cloud. Consequently, the point dipole approximation may be not valid at such a distance. On the other hand, at large distance ($r \gg R_0$) the contribution of the electric charges induced in the conductive layer of the Earth to the total electric field should be taken into account. The charge distribution becomes dipole because of the electric images of charges situated in the explosive cloud. Thus the dipole approximation may be sufficient to explain the electric field generated by the chemical explosion in air.

[4]   We emphasize that systematic investigation of the signal attenuation with distance has not been carried out in previous work. One of the goals of this paper is to study the distance dependence of the explosive-induced electromagnetic field.

[5]   There are many hypotheses concerning the origin of charges caused by an explosion: They might arise because of gas ionization and different mobility of positive and negative charged particles [*Kolsky*, 1954]; they might be created as a result of electrification of scattered explosion

Table 1. Contact Explosions: Characteristics of the High Explosive Charges, Ground, and Emplacement of the Sensors[a]

Event	Mass of High Expl., kg	Explosive	Ground	Emplacement of Sensors			
				Electric Field Sensors		Magnetic Field Sensors	
				Distance R, m	Component	Distance r, m	Component
1–2	0.001	KD-8C	wood plate on the ground	2.5; 4.4	E_z	2.5; 4.4	B_z, B_r, B_θ
3	0.25	ammonite	sandy loam	10; 15; 20; 25	E_z	5	B_z, six sensors
4	0.25	ammonite	sandy loam	10	E_z, four sensors	5	B_z, six sensors
5	0.7	TH 50/50	sandy loam	5; 12	E_z	5; 12	B_z, B_r, B_θ
6	0.7	TH 50/50	sandy loam	15; 20; 25; 30	E_z	10; 5	B_z, B_r, B_θ
7	2	TH 50/50	sandy loam	15; 42	E_z	15; 25	B_z, B_r, B_θ
8–9	3	TNT	marble platform	15; 20; 25; 30	E_z	10; 5	B_z, B_r, B_θ
10	4.2	TNT	granite	16.5; 26.5; 36.5; 46.5	E_z	16.5	B_r
11–12	5	TNT	granite	19; 20 24; 25 29; 30 49; 50	E_z E_z E_z E_z	19; 20	B_z, B_r, B_θ
13–16[b]	5	TNT	granite				
17–18	5	TNT	granite	20.5; 21.5 (0°) 20.5; 21.5 (45°) 20.5; 21.5 (90°) 25.5; 26.5 (0°)	E_z E_z E_z E_z	16.1; 17.1 (0°)	B_z, B_r, B_θ
19	2	TNT	granite	21.2; 26.2; 31.2; 41.2; 51.2; 61.2	E_z	21.2	B_z, B_r, B_θ
20	2	TNT	granite	18; 28; 38; 48; 58; 68	E_z	18	B_z, B_r, B_θ
21	50	TNT	granite	45.2; 55.2; 65.2; 85.2	E_z	45.2	B_r

[a] Zero degrees corresponds to the east (090°) direction from a high explosive charge.
[b] Emplacement of sensors are similar to events 10–12.

products [*Gorshunov et al.*, 1967]; or they might arise because of polarization of the ionized explosion area in the geoelectric field. The effect of the contact between the conductive cloud of explosion products and the Earth was considered by *Cook* [1959]. *Boronin et al.* [1990a, 1990b] explained some characteristics of the experimental waveforms by spatial separation of electric charges resulting from solid particles (e.g., carbon black) moving through gaseous explosion products and oscillations of the explosion products relative to the solid particles.

[6] The influence of the explosive blasting method was investigated by *Gorshunov et al.* [1967]. There it was noted that when blasting is initiated with an electric detonator, currents and charges in lead wires exert a significant influence on the shape of the electric signal. Electric pulses generated by electric detonators used in blasting have been studied by *Brovkin et al.* [1990]; they found that a typical signal has the shape of a pulse with a steep leading edge and a total duration of a few microseconds. A significant increase of the pulse amplitude occurs when the detonator body is magnetized prior to detonation. This phenomenon is caused by shock demagnetization of the ferromagnetic components during the destruction of the detonator body. In the case of group blasting of electric detonators, these results show that detonator failures can be detected and counted at a distance. Use of nonelectrical cap-and-fuse blasting ensures that electric noise from current circuits of the detonator will be eliminated.

[7] In the case of shallow buried chemical explosions, electric fields may also be formed by the processes of electric charge development when explosion products con-tact the rock medium and when explosion products break through cracks in the excavating bowl [*Adushkin and Soloviev*, 1996; *Adushkin et al.*, 1990]. Another effect is electric signal generation by the explosion air wave as it disturbs the charged aerosol concentration in the lower atmosphere [*Soloviev and Surkov*, 1994]. Another factor to consider is that magnetic fields have also been observed from large-scale underground explosions [*Sweeney*, 1989].

[8] Mechanisms of electromagnetic field generation by contact explosions are as yet unknown, and no systematic simultaneous measurements of electric and magnetic field have been made until now. In this paper we present results of such measurements and a theoretical model that adequately describes some of the observed effects.

2. Experimental Program and Instrumentation

[9] To investigate the generation of the electromagnetic field from explosions on the surface, a series of experiments were carried out. High explosive charges of various sizes and types were detonated while electric and magnetic measurements were made at a variety of distances. Characteristics of the high explosive charges, ground surface beneath the charge, and configuration of the sensors are listed in Table 1.

[10] Explosions were detonated directly on the ground surface (sandy loam), on wooden plates, on marble platforms, or directly on a surface of natural granite. The different surfaces were used to investigate the effects on the measured electromagnetic fields of the type and amount of debris mobilized by the explosion. In most cases, repeat

explosions of the same size were carried out to check consistency of the results. Sensors were placed at different distances and oriented along geographic coordinates (e.g., north, east).

[11] In the first series (events 1–9 in Table 1) the explosives were made from trotyl-hexogen 50/50 (ammonite and TNT) with masses of 0.25, 0.7, 2, and 3 kg. Experiments 1 and 2 were designed to observe electromagnetic effects of detonators. For experiments 3–9 the explosives were placed directly on the ground or on a marble block platform which was 0.4 m square and 0.2 m thick. The upper surface of the ground consisted of loam soil. Density of the soil was $(2.6–2.7) \times 10^3$ kg/m^3 with water saturation (by weight) of 8.5–18.5%. The marble blocks were placed in the soil with their top surface level with the ground surface. The explosive was then placed on the marble block surface. For this series the marble blocks were entirely destroyed by the explosion and craters were formed in the soil.

[12] In the second series (events 10–21 in Table 1), TNT charges with masses of 2 and 50 kg were used, placed on a natural granite bedrock base. In this case there was spallation damage of the granite surface, and a small explosive crater was formed.

[13] The vertical component of the electric field strength, $E_z(t)$, and three components of the magnetic induction field, **B**, were recorded from locations above the ground surface during the experiments. Arrival of the seismic waves and airwave generated by the explosion was registered by accelerometers placed on the ground next to the **E** and **B** field recording sites. Type 4170 B&K accelerometers and 2651 charge amplifier were used in our experiments. All electromagnetic sensors and the explosion epicenter were placed along a direct line passing from east to west. This line coincides with the x axis reference used in the theoretical analysis below. The projections of vectors **E** and **B** will be positive if they coincide with the positive direction of x, y, z axes. The recording consistency of the whole group of electrometers and magnetometers was tested by placing the sensors close together at the same distance while an explosion took place (events 3 and 4 in Table 1); differences in the sensor readings were not greater than 20%.

[14] The vertical electric field sensors used are passive electric antennas connected to a sensitive instrumental amplifier and filters [Baryshev, 1995; Ogawa, 1973]. These electrometers, designed for a frequency band of 1 Hz to 10 kHz, have three output terminals (connectors) with amplification factors in the ratio of 1:10:100. The most sensitive third terminal has a response of about 2600 mV/(V/m) and a frequency band from 15 Hz to 10 kHz. Combined use of all terminals provides registration of the electric field strength from at least from 1 mV/m to 2000 V/m; this is needed to study the distance dependence of the amplitude of the electromagnetic signal.

[15] The coil-induction magnetometers for the three-component **B** field measurements consist of a magnetic sensor, preamplifier, integrator, and amplifier and filter circuits. The coil, with a high μ metal core and preamplifier, is placed in a cylindrical waterproof case which is connected to the electronic unit by a cable. The magnetometers, with a frequency passband of 60 Hz to 1.5 kHz, have a response of ~20 mV/pT for peak amplification. A

narrow-band rejecter filter is placed in the magnetometers as well as in the electrometers to provide an industrial noise suppression of 50 Hz. In some experiments we used additional magnetometers with passband of 500 Hz up to 10 kHz and sampling frequency up to 50 kHz. Results of these experiments showed that the shape of the electromagnetic signals did not change significantly when sampling frequency was increased from 10 to 50 kHz.

[16] A notebook computer was used to acquire and digitally store signals of the magnetic and electric field using a 12-bit analog-to-digital converter; the converter allows synchronous multichannel input of analog signals at sampling rates up to 500 kHz per channel. The sampling frequency used was 10–20 kHz, depending on the number of recording channels. Input signals were selected in the range ±5.12, ±2.56, and ±1.024 V. Batteries provided a self-contained power supply of the acquisition system, sensors of the electric and magnetic fields, and accelerometers.

[17] In order to avoid any possible signal contribution from electric detonators, we used the (nonelectric) cap and fuse method for detonation for experiments 3–21 listed in Table 1. We decided to also study the electromagnetic contribution of a common type of nonelectric detonator used in Russia. Two type KD-8C detonators were detonated without explosives (events 1 and 2) with electric and magnetic sensors placed at 2.5 and 4.4 m away. The maximum electric field signal recorded occurred ~0.6 ms after the detonation time and had a magnitude of ~16 V/m and ~3.5 V/m at distances 2.5 and 4.4 m, respectively. The signal of the magnetic field was not distinct from natural background. On the basis of these results, we would expect that the electric signals from this type of detonator will be small at the distances 15–85 m, where electromagnetic signals were measured for our experiments.

[18] Timing of the high explosive charge detonation was defined with the help of an optical sensor consisting of an optical cable ~50 m in length, photoreceiver, and amplifier. One of the optical cable ends was mounted next to the detonator. The light impulse of the explosion was converted to a rectangular electrical signal with duration ~1 s. The leading edge of this signal lasted ~10^{-6} s after the beginning of high explosive charge detonation. The acquisition system of electromagnetic signals was adjusted to a pretrigger mode and was started by the leading edge of the rectangular signal from the optical sensor. Usually, we recorded 1000 samples before and 10,000 samples after the moment of the detonation.

3. Experimental Results

[19] Figures 1, 2, and 3 show representative records of the electric and magnetic field generated by the detonation of high explosive charges on the ground surface. We have chosen, from the first and second series of experiments listed in Table 1, characteristic events which are discussed in detail below. Figure 1 shows representative records of the electric field, $E_z(t)$, three components of the magnetic field (vertical, B_z, tangential, B_θ and radial, B_r) and the vertical component of the ground acceleration for an explosion with a mass of 5 kg (event 12). The accelerometers were placed on the ground surface at distances 28 m from the epicenter. It is obvious from Figure 1h that no ground motion occurs at
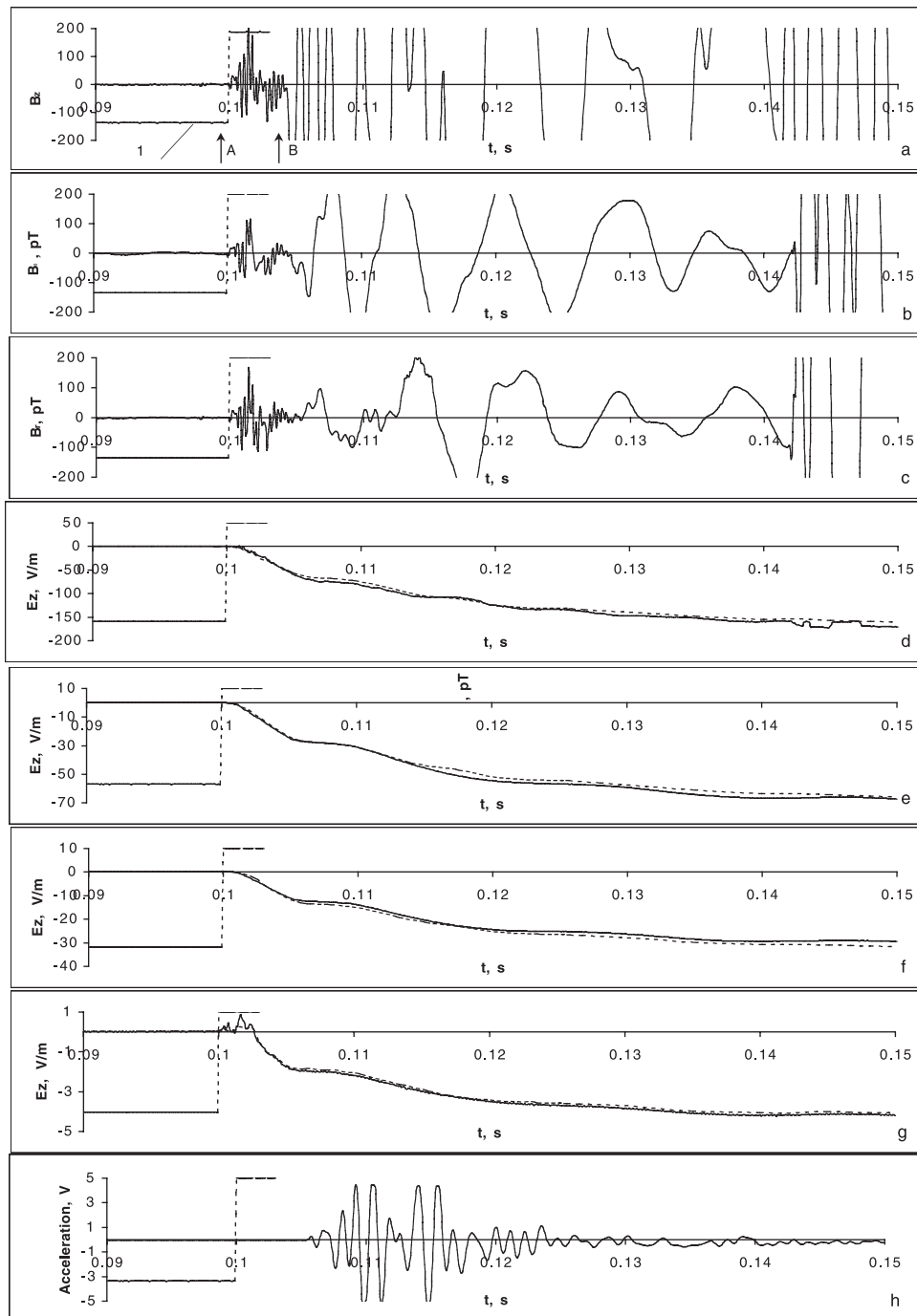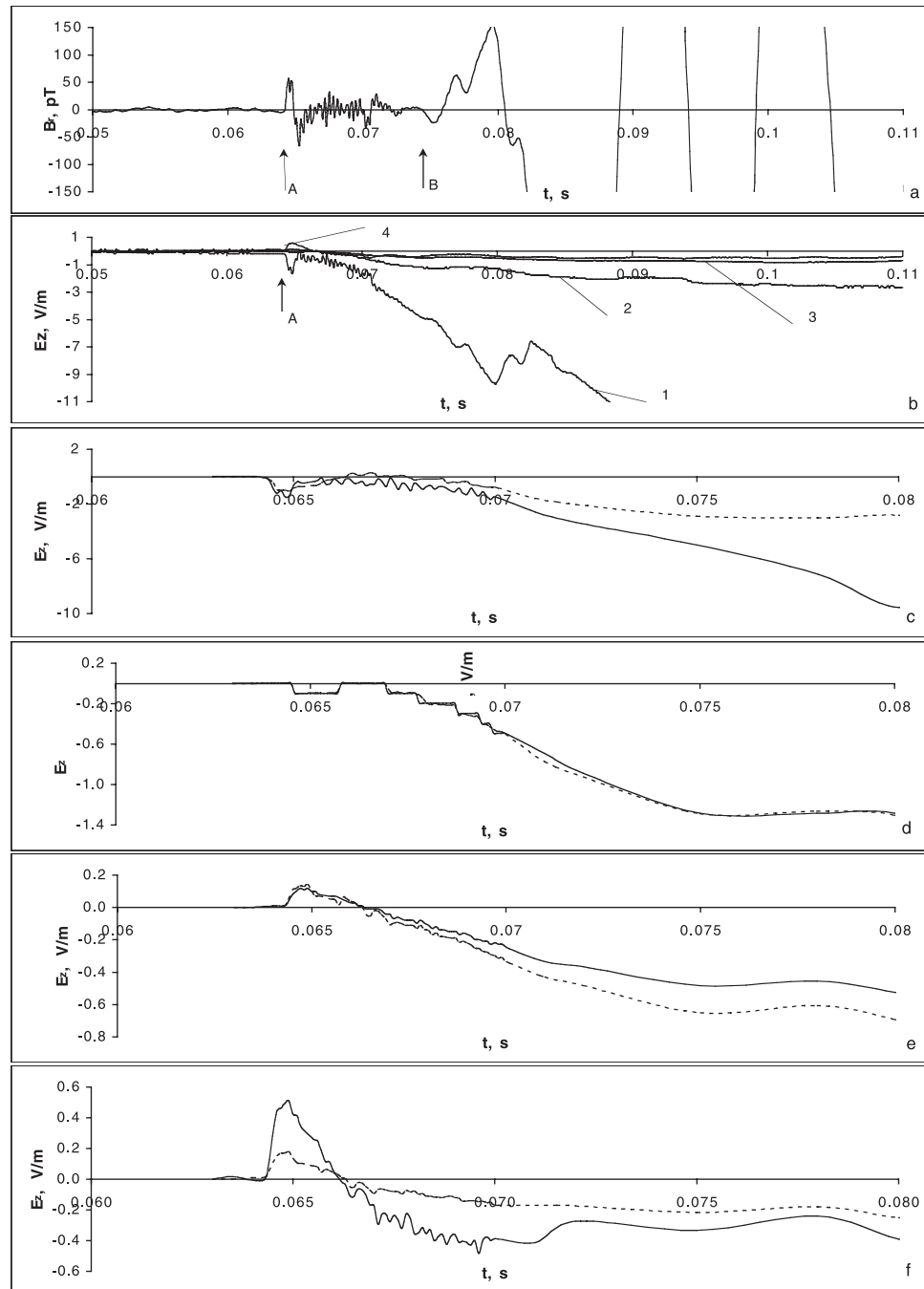
Figure 1. Electromagnetic signals recorded during small-scale explosion with mass of 5 kg (event 12 in Table 1). (a) Vertical magnetic field component, $B_z(t)$, at 20 m distance from epicenter; A, detonation time; B, time associated with arrival of seismic wave; curve 1, rectangular electrical signal from the optical sensor. (b) Tangential magnetic field component, $B_\theta(t)$, at 20 m distance from epicenter. (c) Radial magnetic field component, $B_r(t)$, at 20 m distance from epicenter. (d, e, f, g) Vertical electric field component, $E_z(t)$, at 20, 25, 30, and 50 m distance from epicenter, respectively. $E_z(t)$ obtained from the model is shown by dashed line. (h) Vertical acceleration component at 28 m distance from epicenter.

the sensors at the time the electromagnetic signals are observed. It also appears that an electrical signal originating at the base of the weathered layer, as observed by *Martner and Sparks* [1959] probably does not arrive before the ground motion; such a signal would be expected to have a delay >10 ms (for a 2 km/s seismic velocity and a

weathered zone at least 20 m deep, based on observations at the experimental site). Time in Figures 1–3 is measured from the start of the analog-to-digital converter and recording. The explosion detonation time is marked in Figure 1 by a vertical arrow and corresponds to 0.1 s (the sampling frequency was 10 kHz) from start of the record.
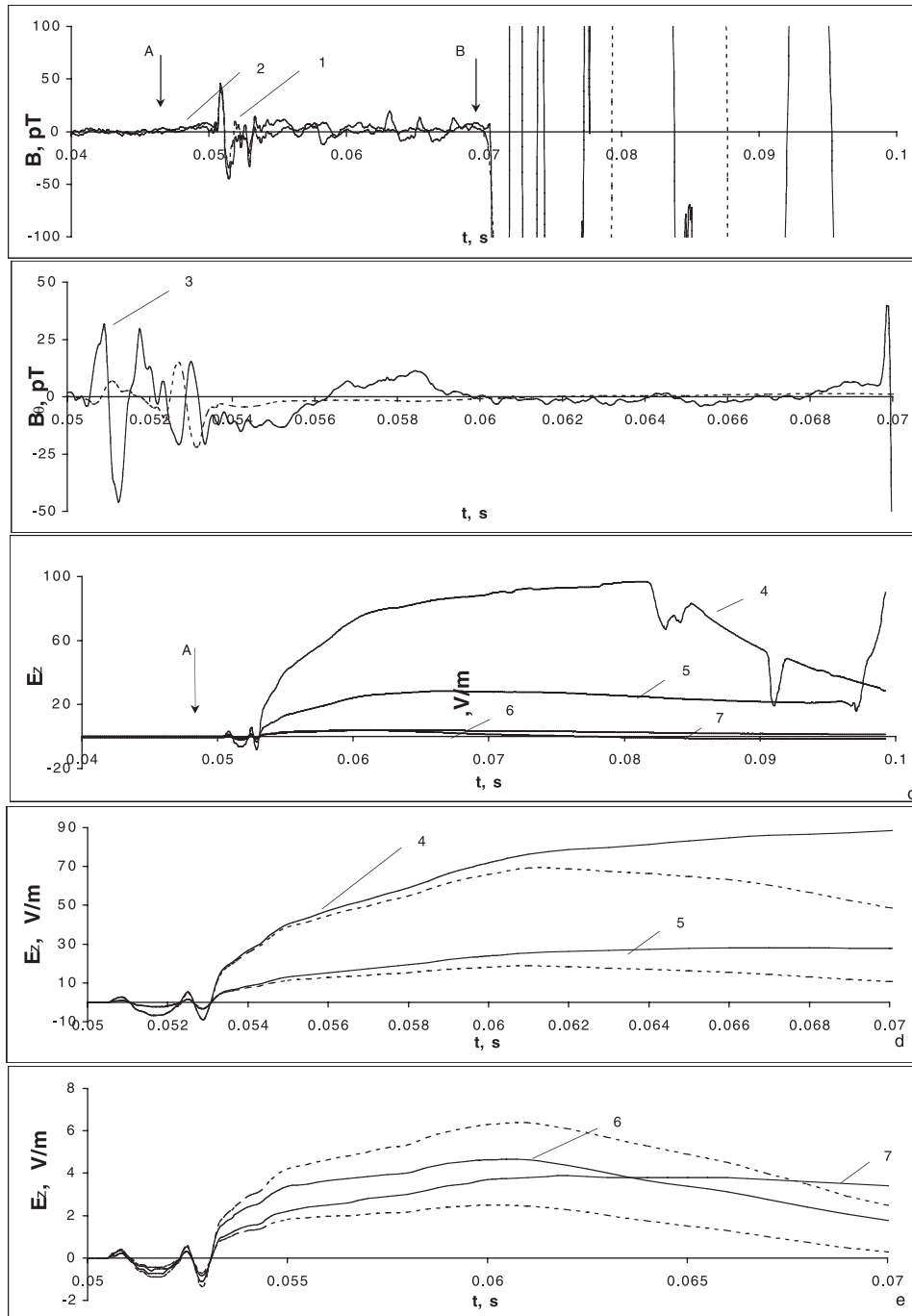
Figure 2. Electromagnetic signals recorded during small-scale explosion with mass of 3 kg (event 8 in Table 1). (a) Vertical magnetic field component, $B_z(t)$ (curve 1), and radial magnetic field component, $B_r(t)$ (curve 2), at 10.5 m distance from epicenter; A, detonation time; B, time associated with arrival of seismic wave. (b) Tangential magnetic field component, $B_\theta(t)$, (curve 3) at 10.5 m distance from epicenter; $B_\theta(t)$ obtained from the model is shown by dashed line. (c) Vertical electric field component, $E_z(t)$, at different distances from epicenter; curve 4, 15 m distance; curve 5, 20 m distance; curve 6, 25 m distance; curve 7, 30 m distance. (d) Vertical electric field component, $E_z(t)$, at different distances from epicenter; curve 4, 15 m distance; curve 5, 20 m distance; curve 6, 25 m distance. $E_z(t)$ obtained from the model is shown by dashed line. (e) Vertical electric field component, $E_z(t)$, at different distances from epicenter; curve 6, 25 m distance; curve 7, 30 m distance. $E_z(t)$ obtained from the model is shown by dashed line.

Figure 3. Electromagnetic signals recorded during small-scale explosion with mass of 50 kg (event 21 in Table 1). (a) Radial magnetic field component, $B_r(t)$, at 45.2 m distance from epicenter; A, detonation time; B, time associated with arrival of seismic wave. (b) Vertical electric field component, $E_z(t)$, at different distances from epicenter; curve 1, 45.2 m distance; curve 2, 55.2 m distance; curve 3, 65.2 m distance; curve 4, 85.2 m distance. (c, d, e, f) Vertical electric field component, $E_z(t)$, at different distances of 45.2, 55.2, 65.2, and 85.2 m from epicenter, respectively. $E_z(t)$ obtained from the model is shown by dashed line.

[20] Representative records of the electric field, $E_z(t)$, and three components of the magnetic field, B_z, B_r, B_θ, for the explosion with a mass of 3 kg (event 8) are shown in Figure 2. Event 9 was a repeat of event 8 with the same size charge; it resulted in electric and magnetic field signals similar to those of Figure 2. For some moments of time, variability of the electric field magnitudes in the different

experiments is ~10%, as can be seen from the data points of Figures 4a and 4b (compare the asterisk and square data); for other moments of time the electric field magnitudes differ much more.

[21] Figure 3 shows representative records of the vertical electric field and radial component of the magnetic field for an explosion with mass of 50 kg (event 21). It is obvious
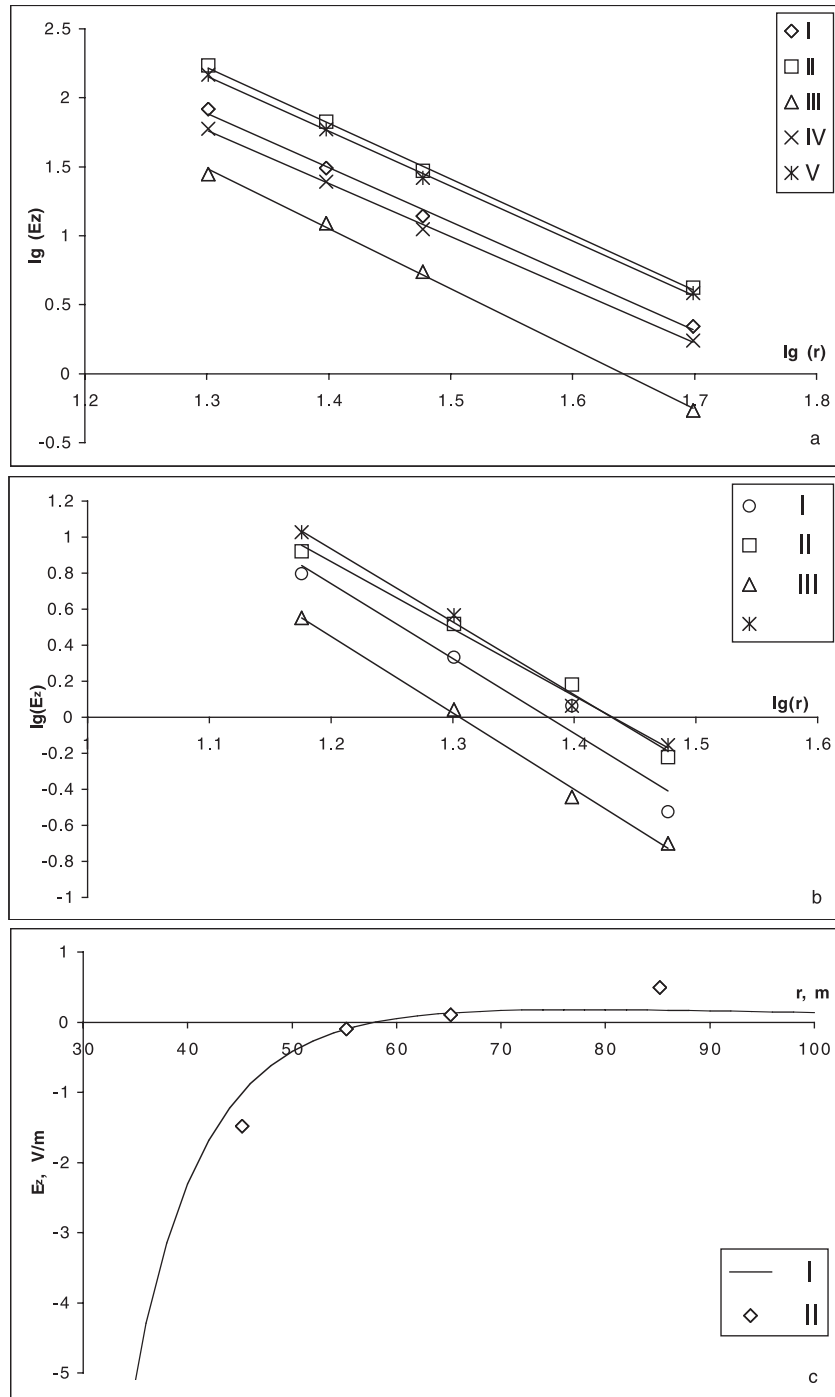
Figure 4. (a) Absolute values of electric signals versus distance r for the contact explosion with mass of 5 kg (event 12 in Table 1). I, II, III, IV, and V are magnitudes corresponding to times 0.103, 0.105, 0.110, 0.130, and 0.150 s for signals that are shown on Figures 1d–1g. (b) Absolute values of two initial peaks of electric signals versus distance r for the surface explosion with mass of 3 kg. I and II are magnitudes corresponding to time 0.0517 and 0.0529 s for signals that are shown on Figure 2c. III and IV are magnitudes corresponding to time 0.0516 and 0.05275 s for signals recorded during the second explosion with a mass of 3 kg (event 9 in Table 1). (c) Value of the initial peak of the electric signal versus distance r for the explosion with mass of 50 kg (event 21 in Table 1). I is relation (2). II is magnitude corresponding to time 0.0648 s for signals that are shown on Figure 3b.

Table 2. Empirical Constants a and b From the Relation $\log(E_z) = -a \log (r) + b$ That Approximates Variations of Absolute Values of the Magnitude, E_z, With Distance r

Event	Time After Detonation, ms	A	b
3	0.5; 1.7; 4; 6	3.0; 3.2; 3.2; 3.1	3.8; 4.8; 4.6; 4.4
6	2.35; 4.2; 6.2; 12	3.8; 4.1; 4.6; 3.8	5.4; 6.0; 6.5; 5.8
8	1.7; 2.9; 5; 10	4.2; 3.7; 4.4; 4.6	5.6; 5.3; 6.8; 7.3
9	1.6; 2.75; 5; 11	4.3; 4.1; 4.1; 4.1	5.7; 5.8; 6.2; 6.5
10	2; 5; 10; 17	3.5; 4.1; 4.2; 4.7	5.3; 6.7; 6.6; 7.4
11	3; 5; 10; 30; 50	4.1; 4.6; 4.0; 4.1; 4.1	6.4; 7.5; 6.9; 7.3; 7.4
12	3; 5; 10; 30; 50	4.3; 3.9; 3.9; 4.0; 4.0	7.1; 6.8; 7.0; 7.7; 7.5
19	5; 10; 15; 20	4.0; 4.2; 4.3; 4.0	6.5; 7.1; 7.4; 7.0
20	5; 10; 15; 20	4.0; 4.1; 4.1; 4.2	6.4; 6.7; 6.9; 7.1

from Figures 1–3 that the signals are low-frequency in character. The oscillation period of the fields is equal to several milliseconds. Electric and magnetic disturbances arise practically simultaneously. Signal magnitudes might reach tens of V/m and pT, respectively. In some experiments the shapes of the electric field signals are similar at different distances from the epicenter (Figures 2c–2e). Sometimes a change of polarity of the initial spike of the electric field signals is observed at different distances from the explosion (Figure 3). The magnetic signal has higher frequency oscillations. In some cases (Figure 2a), the radial and vertical components of the magnetic field are similar to each other. Note also that for the cases of detonations on granite bedrock, there is no weathered zone and an electroseismic effect [*Martner and Sparks*, 1959] would not be expected.

[22] In the first and second series the decrease in the amplitude of the vertical component of the electric field with the distance, r, was investigated. To do this, four or six sensors of the electric field were placed at different distances on a direct line passing through the explosion epicenter. In the case of the contact explosion with mass of 3 kg, the signals were oscillatory, so we used the absolute values of signals to measure amplitude. Magnitudes of two peaks at times $t_1 = 0.0517$ s and $t_2 = 0.0529$ s (Figure 2c) for the first explosion (event 8) and $t_3 = 0.0516$ s and $t_4 = 0.05275$ s for the repeated explosion (event 9) were used for this analysis. Corresponding variations of absolute values of the magnitudes with distance are shown in Figure 4b in logarithmic scale. The value of E_z is measured in V/m here, and r is measured in meters. These relations can be approximated as

$$\log (E_z) = -a \log (r) + b,$$

where empirical constants a and b for the curves 1, 2, 3, and 4 have the following values: $a = 4.2, 3.7, 4.3,$ and 4.1 and $b = 5.6, 5.3, 5.7,$ and 5.8, respectively.

[23] Figure 4a shows variations of absolute values of the signals magnitudes for the explosion with mass of 5 kg (event 12). Magnitudes at times $t_1 = 0.103$ s, $t_2 = 0.105$ s, $t_3 = 0.110$ s, $t_4 = 0.130$ s, and $t_5 = 0.150$ s were used for analysis. The empirical constants a and b for the curves 1–5 have the following values: $a = 4.3, 3.9, 3.9, 4.0,$ and 4.0 and $b = 7.1, 6.8, 7.0, 7.3,$ and 7.5, respectively. The empirical constants a and b for the other events listed in Table 1 are given in Table 2. The signal amplitude for the events given in Table 2 decreases approximately as the

fourth power of distance. This fact suggests that in these cases, the system of electric charges resulting from the explosion correspond to a quadrupolar, rather than to a dipolar, system at the initial stage of the explosion on the surface. It should be noted that these results only apply within the distance range studied here.

[24] More complex relationships were observed in some experiments. For instance, in the case of the explosion with mass of 50 kg, the polarities of the initial spike of signals recorded at different distances were opposite in sign as shown in Figures 3c–3f. Such dependence is explained below by the presence of dipole as well as quadrupolar moments. Contributions of corresponding terms to the signal are different at different distances.

4. Theory

[25] The low-frequency electromagnetic field of a contact explosion is caused by formation and separation of electric charges. These charges might be contained in the explosion products and in the gas ionized by the shock wave, or they might come from particles of soil. Moreover, electric charges are also induced in the conductive layers of the Earth. These induced electric charges have opposite sign but the same values as charges located in the explosive cloud. These charges should be taken into account in order to make a correct description of explosive-induced electromagnetic field.

[26] At large distances from the explosion epicenter we can use expansion formulas of multipoles. In this case it should be taken into consideration that the quadrupolar term is not small in comparison with the dipole term, at least at the initial stage. In the simplest model of such a system, two effective point charges, q_1 and $-q_2$, replace the charge aggregate in the cloud. Let as assume that the first and the second charges are at heights of h_1 and h_2 from the Earth's surface, respectively. All variables depend on the time t from the detonation. Let us place the origin of Cartesian coordinates at the explosion point on the earth's surface and direct the z axis upward. The projections of the charges will be designated as x_1, y_1 and x_2, y_2, respectively.

[27] For convenience, we also use another coordinate system, x', y', z', with the x' axis passing through the projections of the charges, i.e., $y'_1 = y'_2 = 0$. Moreover, let us assign the coordinates $x'_1 = l/2$ and $x'_2 = -l/2$ to the first and second charges, respectively (Figure 5). The polar radius, $r = (x'^2 + y'^2)^{1/2}$, and an angle θ between radius
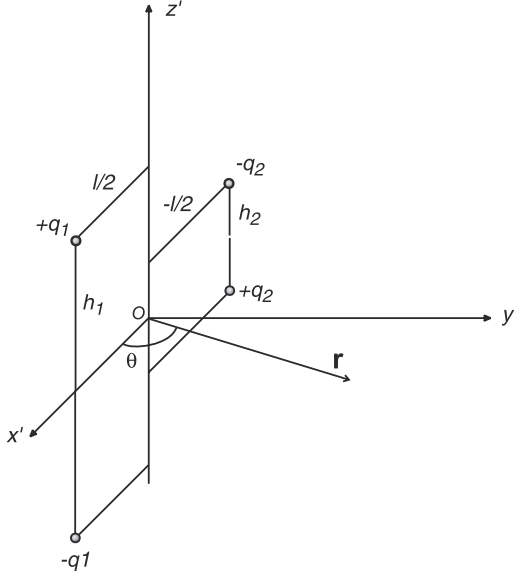
Figure 5. System of coordinates and plan of location of effective electric charges used in the model to estimate electric and magnetic fields.

and the positive direction of x' axis will be entered in the following equations as well. Angle θ is measured from the x axis in an anticlockwise direction. If the charges are in motion, the x' and y' axes of the chosen system of coordinates are displaced and rotate in a horizontal plane. In this case the angle θ and the distance r for each point where the electromagnetic sensors are located depend on time. In essence, only the angle θ needs to be considered as a variable.

[28] We assumed that the Earth is a perfect conductor in order to take into account the field of the charges induced in the Earth. In this case the field is equivalent to the field of the electric images of the charges q_1 and $-q_2$. Only the vertical component of the electric field is not equal to zero on the Earth's surface ($z = 0$):

$$E_z = \frac{q_2 h_2}{2\pi\varepsilon_0 \left(r^2 + h_2^2 + l^2/4 + rl\cos\theta\right)^{3/2}} - \frac{q_1 h_1}{2\pi\varepsilon_0 \left(r^2 + h_1^2 + l^2/4 - rl\cos\theta\right)^{3/2}}, \quad (1)$$

where ε_0 is the dielectric permittivity of free space.

[29] Equation (1) might be simplified for the case of large distances, when $r/l \gg 1$ and $r/h_{1,2} \gg 1$. Then, equation (1) might be expanded in a series per perturbations:

$$E_z(r, \theta, t) = -\frac{p_z(t)}{4\pi\varepsilon_0 r^3} - \frac{D'_{xz}(t)}{4\pi\varepsilon_0 r^4} - \cdots \quad (2)$$

$$p_z = 2(q_1 h_1 - q_2 h_2), \quad D'_{xz} = 3l(q_1 h_1 + q_2 h_2)\cos\theta.$$

Here p_z is the projection of the dipole moment onto the z axis. The single nonzero component of the tensor of quadrupole moment of the charge system for the given system of coordinates is marked as D'_{xz}.

[30] In the original coordinates system, x, y, z, equation (2) can be rewritten as

$$E_z = -\frac{p_z(t)}{4\pi\varepsilon_0 r^3} - \frac{yD_{yz}(t) + xD_{xz}(t)}{4\pi\varepsilon_0 r^5} - \cdots$$

$$D_{xz} = D_{zx} = 6(q_1 h_1 x_1 - q_2 h_2 x_2), \quad (3)$$

$$D_{yz} = D_{zy} = 6(q_1 h_1 y_1 - q_2 h_2 y_2).$$

Thus the quadrupolar term is described by two variable components, D_{xz} and D_{yz}, instead of D'_{xz}. It should be noted that equation (3) is more general than was assumed, since this equation can correspond to a random system of charges located above conductive ground. If we take the case where a sensor is placed on the x axis (i.e., the sensor coordinates are $(r, 0, 0)$) by substituting $y = 0$ into equation (3) one can see that the electric field depends on only component D_{xz}. We can then transform D_{xz} using the relations $q_1 h_1 \approx q_2 h_2$ and $x_1 - x_2 = l\cos\theta$, leading to coincidence of the values D_{xz} and D_{xz} belonging to equations (2) and (3).

[31] The experiments showed that at the initial stage the spatial separation of the formed charges is small, i.e., $q_1 h_1 \approx q_2 h_2$. So, the quadrupolar term in equation (2) might be greater than the dipole term at the closest distances. This situation is observed at the distances which satisfy the following requirement:

$$r \ll r_0(t) = \left|\frac{D'_{xz}(t)}{p_z(t)}\right|, \qquad r_0(t) \sim l\frac{q_1 h_1 + q_2 h_2}{q_1 h_1 - q_2 h_2}. \quad (4)$$

Next we estimate the magnetic field arising due to the motion of the charges. The charge coordinates are considered as prescribed time functions. The vector potential $\mathbf{A}$ of the electromagnetic field is

$$\mathbf{A} = \frac{\mu_0}{4\pi}\left(\frac{\dot{\mathbf{p}}}{r} - \frac{1}{6}\nabla \cdot \frac{\dot{\mathbf{D}}}{r} + \nabla \times \frac{\mathbf{M}}{r}\right), \quad (5)$$

where $\mathbf{D}$ is a quadrupole tensor and $\mathbf{p}$ and $\mathbf{M}$ are the electric and magnetic dipole moment vectors of the system, respectively, and μ_0 is magnetic permittivity of free space. An overdot refers to differentiation with respect to time.

[32] Taking into consideration that the quadrupolar moment has only two nonzero components (equation (3)) let us reduce equation (5) to the form

$$A_x = \frac{\mu_0}{4\pi r^3}\left(\frac{z\dot{D}_{xz}}{6} + zM_y - yM_z\right),$$

$$A_y = \frac{\mu_0}{4\pi r^3}\left(\frac{z\dot{D}_{yz}}{6} + xM_z - zM_x\right), \quad (6)$$

$$A_z = \frac{\mu_0}{4\pi r}\left[\dot{p}_z + \frac{1}{r^2}\left(\frac{x\dot{D}_{xz}}{6} + \frac{y\dot{D}_{yz}}{6} + yM_x - xM_y\right)\right].$$

Substitution of equation (6) in the formula $\mathbf{B} = \nabla \times \mathbf{A}$ gives the induction $\mathbf{B}$ of the magnetic field. So the magnetic field components in this point can be written as

$$B_x = \frac{\mu_0 M_x}{2\pi r^3}, \quad B_z = -\frac{\mu_0 M_z}{4\pi r^3}, \quad B_y = \frac{\mu_0}{4\pi r^3}\left(r\dot{p}_z + \frac{\dot{D}_{xz}}{2} - M_y\right). \quad (7)$$

There are several possible mechanisms of the magnetic moment formation. For example, motion of solid charged particles resulted from detonation and ground surface fracture as well as shock-induced current in the ground and conductivity current in ionized gas can contribute to the magnetic signal. Here we estimate the magnetic field caused by motion of the effective charges q_1 and $-q_2$ and their mirror images in the ground. For this case the components of magnetic moments, **M**, are

$$M_x = y_1 \dot{p}_1 - \dot{y}_1 p_1 - y_2 \dot{p}_2 + \dot{y}_2 p_2,$$
$$M_x = x_2 \dot{p}_2 - \dot{x}_2 p_2 - x_1 \dot{p}_1 + \dot{x}_1 p_1, \quad M_z = 0. \tag{8}$$

where $p_1 = q_1 h_1$ and $p_2 = q_2 h_2$. For simplicity we assume the same origin of the coordinate systems x, y and x', y' (Figure 5). It is convenient to present the computing result in polar coordinates r, θ, where θ denotes angle between axes x' and x. Then substitution of equation (8) into (7) leads to

$$B_r = \frac{\mu_0}{4\pi r^3} [(\dot{p}_1 + \dot{p}_2)l \sin\theta + 2(p_2 \dot{y}_2 - p_1 \dot{y}_1)],$$

$$B_\theta = \frac{\mu_0}{4\pi r^3} [r\dot{p}_z + 2(\dot{p}_1 + \dot{p}_2)l \cos\theta + 2(p_1 \dot{x}_1 - p_2 \dot{x}_2)], \quad B_z = 0. \tag{9}$$

On the basis of films of explosions we observe that there are only weak deviations from axial symmetry in the dust clouds and distribution of fractured rock frag ments at the initial stage of the explosion. So, for contact explosions the horizontal velocity of the centers of the electric charge distribution is likely to be significantly less than the vertical velocity. In this case it is possible to neglect the last terms in equation (9). For this case we can also use the following approximation for the derivative of the quadruple moment equation (2): $\dot{D}'_{xz} = 3(\dot{p}_1 + \dot{p}_2)l \cos\theta$.

[33] Then we get

$$B_r = \frac{\mu_0 \dot{D}'_{xz}}{12\pi r^3} \tan\theta, \quad B_\theta = \frac{\mu_0}{4\pi r^2}\left(\dot{p}_z + \frac{2\dot{D}'_{xz}}{3r}\right). \tag{10}$$

If the dipole moment derivative is small, the corresponding term in equation (10) might be eliminated and then both horizontal components of the magnetic field are approximately proportional to each other:

$$B_\theta \approx \frac{\mu_0 \dot{D}'_{xz}}{6\pi r^3}, \quad B_r \approx \frac{\tan\theta}{2} B_\theta. \tag{11}$$

[34] These results were derived for the case of infinite ground conductivity. The case of the finite conductivity ($\sigma = 10^{-2} - 10^{-3}$ S/m) leads to corrections of the order of $\varepsilon_0/(\sigma\tau) \ll 1$, where $\tau \sim 0.01 - 1$ ms is a typical time of the explosion process. Because of their cumbersome form, the corresponding computations are not developed here, but it should be noted that for the case of vertical magnetic moment these corrections could be important.

5. Discussion

[35] When the experimental results presented in Figures 4a and 4b and Table 2 are compared with equation (2), it is apparent that in these experiments the amplitude of the electric field decreases approximately proportional to r^{-4}. This means that the distribution of electric charges resulting from the surface explosion is quadrupolar in the initial stages of the explosion.

[36] Analysis of the relations shown in Figure 4b allows us to estimate the quadrupole moment of the system as $D'_{xz} \approx -(1.3-0.4) \times 10^{-4}$ C m^2. From the experimental data presented by *Adushkin and Soloviev* [1996] the electric charge of products of the surface explosion varies as the 0.65 ± 0.05 power of the explosive mass. On the base of this empirical dependence the charges can be estimated as $q_1 \approx q_2 \approx 2 \times 10^{-6}$ C. The radius of the shock wave front is about 2 m at 2 ms. Let us use this value for h_1 and h_2 in equation (4). Substitution of these values in the equation for the quadrupo le moment gives a characteristic horizontal distance between the charges of $l \approx 2-7$ mm. It should be noted that this is an effective distance between the centers of positive and negative charge distributions.

[37] Such negligible deflection (2–7 mm) from axial symmetry as indicated above might be caused by subtle effects. In particular, asymmetric destruction of the rock or soil surface after detonation time might be a cause of some asymmetry in motion of the explosion products and gas and hence an asymmetry of the electric charge distributions.

[38] The dipole and quadrupole terms in equation (2) were comparable in some experiments. To cite an example, in the case of the explosive with mass of 50 kg, various polarities of the initial peak of the signal were observed at different distances from the explosion, as shown in Figures 3c–3f and 4c. This can be explained by predominance of the quadrupole term at short distances, with the dipole term more significant at large distances because the dipole term decreases more slowly away from the epicenter. It is seen from Figure 4c that both terms of equation (2) were equal at a distance $r_0 \approx 57$ m. Hence it follows that the quadrupole and dipole moments of the charge system might be estimated as $D'_{xz} = -p_z r_0 \sim -4.3 \times 10^{-3}$ C m^2 and $p_z \sim 5.4 \times 10^{-5}$ C m, respectively, at the moment of the peak formation.

[39] Equation (2) has been used to interpolate the experimental time dependencies of signals measured by four electric field sensors placed at different distances from the epicenter. A χ^2 criterion has been applied to calculate the dipole moment and the value of D$'_{xz}$ at each instant of time. The results, presented in Figure 6, were substituted into equation (2). The computed results, shown in Figures 1–3, show that equation (2) is a good approximation to the experimental data. It is also worth notice that the order of magnitude of the values D_{xz} and p_z is in good agreement with the crude estimates described above.

[40] An interesting feature of Figure 6 is that the parameter D'_{xz} reverses sign. Apparently, the value $3l(q_1 h_1 + q_2 h_2)$ cannot reverse sign, so it must be that the angle θ varies with time. One cause of such an effect might be rotation of explosion products and gas over the shock wave front around the vertical axis. If the electric charges are included in this motion, a straight line passing through projections of effective charges q_1 and q_2 rotates too. Its rotation period is estimated from the data (Figures 1–3) as 2–50 ms.
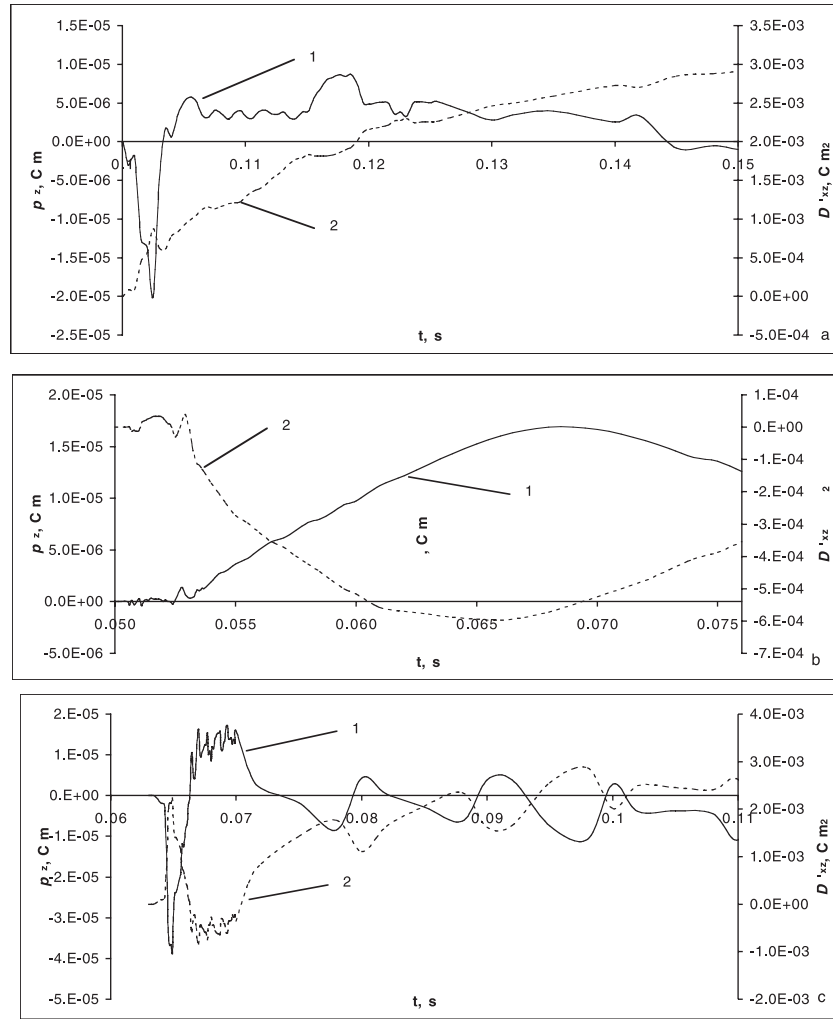
Figure 6. Dipole and quadrupolar moments of the electric charge system versus time. (a) The mass of high explosive is 5 kg (event 12 in Table 1). Curve 1, dipole moment $p_z(t)$ (left scale); curve 2, quadrupolar moment $D'_{xz}(t)$. (b) The mass of high explosive is 3 kg (event 8 in Table 1). Curve 1, dipole moment $p_z(t)$ (left scale); curve 2, quadrupolar moment $D'_{xz}(t)$. (c) The mass of high explosive is 50 kg (event 21 in Table 1). Curve 1, dipole moment $p_z(t)$ (left scale); curve 2, quadrupolar moment $D'_{xz}(t)$.

[41] If the electrical charges are separated in a horizontal plane, angular distribution of the electric field implies that an azimuthal change in the polarity (sign) of the field could be observed. This is embodied by the $\cos\theta$ in the quadrupolar term of equation (2). Various polarities of the initial peak of the electric field signal will be observed at different directions from the explosion. For directions differing by 180° the electric field signals could have opposite sign. In future experiments we intend to investigate the character of the dependence of signals on direction in order to check the correctness of this proposed model for the spatial charge distribution.

[42] Motion of the charges might be a cause of magnetic fields registered in the experiments. First, let us give crude estimations of the magnetic fields based on equations (9) and (10). It should be taken into account that $dD'_{xz}/dt \sim D'_{xz}/\tau$ as an order of magnitude, where the characteristic time τ might be evaluated from Figure 2b. The magnetic field oscillates irregularly with a "period" of ~5 ms, but the leading edges of some peaks have a duration of ~2 ms, so it is

reasonable to use $\tau \approx 2$ ms. At a distance $r = 10.5$ m, where the magnetometer was placed, and $\theta = \pi/4$ we have $B_\theta \approx (12-39)$ pT and $B_r \approx (6-20)$ pT. These estimates correspond to the experimental data of Figure 2b which show amplitudes of B_θ and B_r of up to 40 pT.

[43] To obtain more precise estimation of B_θ, the functions $D'_{xz}(t)$ and $p_z(t)$ obtained above and presented in Figure 6 have been used. In this case, the procedure of numerical differentiation was applied to $D'_{xz}(t)$ and $p_z(t)$. Comparison of experimental and theoretical data (Figure 2b) shows that "oscillation" trains originate in both cases at the same time. On the other hand, these oscillations have different amplitudes and phases. Thus we need to consider the presence of additional sources for the magnetic field variations.

[44] The model suggested in this paper gives an adequate description of the electric field observed after explosions. It is possible to suppose that electric field and at least part of the magnetic fields generated by a contact explosion have the same source: moving charges connected with the ion-

ized gas, explosion products, and debris. The possibility of other mechanisms of magnetic field generation must not be ruled out. Observations of a nonzero vertical component of magnetic field contradict the theory developed here.

[45] If the formation and motion of electrical charges in the area of the explosion is a basic mechanism of electromagnetic signals generation both for small-scale and large-scale chemical explosions, at least at the early stage; this feature will help to distinguish electromagnetic parameters of chemical and nuclear explosions because there are several additional mechanisms of electromagnetic field generation for nuclear explosions (such as the mechanism of geomagnetic field exclusion, or "magnetic bubble").

[46] Another important result is contained in these experiments which must be taken into consideration when considering large-scale surface explosions. The experiments showed the existence of two zones (near and far) that differ from each other by the dependence of low-frequency electromagnetic field amplitude decreasing with distance where amplitude decreases as r^{-4} near the explosion epicenter, where $r < r_0$, and as r^{-3} outside of this area. As follows from the experimental data of *Adushkin and Soloviev* [1996], the vertical separation of electric charges and dipole moment increase with time. The observed electric field has dipole type when the time is greater than $1-10$ s. These data support our calculations and suggestion that the critical distance $r_0 \sim |D_{xz}/p_z|$ decreases with time.

[47] Results of the experiment may be very different for the cases of the two zones mentioned above; that is, the experimental data depend on where the observation point is located with respect to the moving cloud of explosion products and debris. It is possible to suppose that such dependence is also applicable for large-scale explosions.

6. Conclusions

[48] The main results of this work are the following:

1. Experimental results and the analysis carried out above show that the electric and magnetic fields, arising prior to arrival moment of seismic and acoustic air waves, are produced by detonation of high explosive charges on the ground surface.

2. Generation of the electromagnetic field from the contact explosion can be explained from a theoretical point of view by formation and motion of electrical charges in the area of the explosion and in conductive layers of the Earth. It is possible that such charges are due to ionization of gas and explosion products as well as from electrification of scattered rock and soil fragments.

3. The electromagnetic field of the contact explosion has a quadrupole character, at least in the initial stage of the explosion. Its amplitude decreases with distance, r, approximately as r^{-4}.

4. Such r^{-4} dependence is applicable in an area limited by some critical radius, r_0, which depends on time. The field amplitude decreases as r^{-3} in the area where $r > r_0$ and the dipole term predominates.

5. Results of measurements of the electromagnetic field from explosions may be significantly different for the two regions: near zone ($r < r_0$) and far zone ($r > r_0$); that is, the experimentation data depend on where the observation point is located. This fact should be taken into consideration when

comparing small- and large-scale explosions and distance to measurement point.

6. It is likely that the horizontal separation of positive and negative charges in space will behave randomly. Effective charges may rotate around the vertical axis because of vortexes arising beyond the shock front.

7. In the experimental records, the fact that the vertical and horizontal components of the magnetic field are of the same order of magnitude conflicts with the theory developed here. This implies that another mechanisms of magnetic field generation can contribute to the total magnetic signal.

References

Adushkin, V. V., and S. P. Soloviev, Generation of low-frequency electric fields by explosion crater formation, *J. Geophys. Res.*, *101*, 20,165–20,173, 1996.

Adushkin, V. V., S. P. Solovev, and V. V. Surkov, Electrical field arising during ejection explosion, *Combust. Explos. Shock Waves*, *26*, 478–482, 1990.

Baryshev, V. I., The method of symmetrical fields for potential gradient measurements in a weak conduction medium (in Russian), in *Dynamic Processes in Internal and External Environments of the Earth*, pp. 167–174, Inst. for the Dyn. Of the Geosphere, Russ. Acad. of Sci., Moscow, 1995.

Boronin, A. P., J. A. Medvedev, and B. M. Stepanov, Electrical impulse and dynamics of the explosive products expansion (in Russian), *Phys. Combust. Explos.*, *9*, 541–551, 1973.

Boronin, A. P., V. N. Kapinos, S. A. Krenev, and V. N. Mineev, On a physical mechanism of electromagnetic field generation by the explosion of condensed explosives charges: Literature review (in Russian), *Phys. Combust. Explos.*, *26*, 110–116, 1990a.

Boronin, A. P., V. N. Kapinos, and S. A. Krenev, On a physical mechanism of electromagnetic field generation by the explosion of condensed explosives charges: The results of the experimental studies (in Russian), *Phys. Combust. Explos.*, *26*, 117–123, 1990b.

Brovkin, Y. V., S. Z. Dunin, A. P. Popryadukhin, V. V. Surkov, and I. N. Tochkin, Recording of the number of explosions by electromagnetic methods, *J. Min. Sci.*, *26*, 522–526, 1990.

Cook, M. A., *The Science of High Explosive*, 440 pp., Reinhold, New York, 1959.

Gertcenshtein, M. E., and E. I. Sirotinin, The nature of electric pulse of explosion (in Russian), *J. Appl. Mech. Tech. Phys.*, *2*, 72–75, 1970.

Gorshunov, L. M., G. P. Kononenko, and E. I. Sirotinin, Electromagnetic disturbances under explosion (in Russian), *J. Exp. Theoret. Phys.*, *53*, 818–821, 1967.

Kolsky, H., Electromagnetic waves emitted on detonation of explosives, *Nature*, *173*, 77, 1954.

Martner, S. T., and N. R. Sparks, The electroseismic effect, *Geophysics*, *24*, 297–308, 1959.

Ogawa, T., Analysis of measurement techniques of electric fields and current in atmosphere, *Contrib. Geophys. Inst. Kyoto Univ.*, *13*, 111–137, 1973.

Soloviev, S. P., and V. V. Surkov, Electric perturbations in the atmospheric surface layer caused by an aerial shock wave, *Combust. Explos. Shock Waves*, *30*, 117–121, 1994.

Sweeney, J. J., An investigation of the usefulness of extremely low-frequency electromagnetic measurements for treaty verification, *Rep. UCRL-53899*, Lawrence Livermore Natl. Lab., Livermore, Calif., 1989.

———————————

S. P. Soloviev, Institute of Geospheres Dynamics, Leninsky Prospect, 38 Korpus 6, 117334 Moscow, Russia. (soloviev@idg.chph.ras.ru)

V. V. Surkov, Moscow State Engineering Physics Institute, MEPhI, 31, Kashirskoye Road, 115409 Moscow, Russia. (surkov@redline.ru)

J. J. Sweeney, Lawrence Livermore National Laboratory, P.O. Box 808, L-208, Livermore, CA 94550, USA. (sweeney3@llnl.gov)